nature structural & molecular biology

Iron-regulatory proteins limit hypoxia-inducible factor-2α expression in iron deficiency

Mayka Sanchez[1–3], Bruno Galy[2], Martina U Muckenthaler[1–4] & Matthias W Hentze[1,2,4]

Hypoxia stimulates erythropoiesis, the major iron-utilization pathway. We report the discovery of a conserved, functional iron-responsive element (IRE) in the 5′ untranslated region of the messenger RNA encoding endothelial PAS domain protein-1, EPAS1 (also called hypoxia-inducible factor-2α, HIF2α). Via this IRE, iron regulatory protein binding controls *EPAS1* mRNA translation in response to cellular iron availability. Our results uncover a regulatory link that permits feedback control between iron availability and the expression of a key transcription factor promoting iron utilization. They also show that an IRE that is structurally distinct from, for example, the ferritin mRNA IRE and that has been missed by *in silico* approaches, can mediate mechanistically similar responses.

In biology, iron can occur in two valency states, ferrous (2+) and ferric (3+). This characteristic allows it to reversibly bind oxygen, a property underlying oxygen transport by hemoglobin in circulating erythrocytes. The number and hemoglobin content of erythrocytes is a major determinant of both tissue oxygenation and iron utilization, and mammals respond to hypoxia with increased erythropoiesis and duodenal iron absorption[1,2].

Mammals adapt to changes in oxygen availability through a response pathway mediated by the transcription factor hypoxia-inducible factor-1 (HIF1 in human). HIF1 was initially described as a 'basic helix-loop-helix/Per-Arnt-Sim homology' (bHLH-PAS) heterodimer composed of the oxygen-regulated HIF1α subunit and the constitutively expressed ARTN (also called HIF1β) subunit[3]. HIF2α is a close homolog of HIF1α and also forms a functional heterodimer with ARNT[4–7]. HIF2α is referred to by various names in the literature (as HIF2α[8], HIF-like factor (HLF)[4], HIF-related factor (HRF)[5] or member of PAS superfamily-2 (MOP2)[6]); we will refer to it by its official name, EPAS1 (ref. 7). The HIFα proteins respond to changes in oxygen tension indirectly through hydroxylation-dependent changes in protein stability and activity[9]. Under normoxia, the HIFα proteins are hydroxylated on two conserved proline residues, promoting their association with the von Hippel–Lindau (VHL) ubiquitin ligase and subsequent proteasomal degradation, leading to a very short half-life[10]. In addition, hydroxylation of a conserved asparagine residue in the HIF1α and EPAS1 C-terminal transactivation domains impairs their interaction with the transcriptional coactivator p300, switching off the activity of remaining HIFα proteins[11]. Hypoxia abrogates HIFα hydroxylation, resulting in increased protein stability and activity. HIF1 regulates more than 40 genes involved in angiogenesis, vascular reactivity and remodeling, glucose and energy metabolism, cell proliferation and survival, erythropoiesis and iron homeostasis through hypoxia response elements (HREs; for a review, see ref. 12). Although HIF1α and EPAS1 transcriptionally regulate a common set of genes, specific target genes for EPAS1, such as the erythropoietin and TGFα genes, have been identified[13–15].

Cellular iron metabolism is coordinately controlled by the iron regulatory proteins IRP1 (also called ACO1) and IRP2 (also called IREB2). IRPs bind IREs, *cis*-regulatory RNA motifs present in the untranslated regions (UTRs) of mRNAs encoding proteins of iron acquisition (transferrin receptor-1, TFRC, also called TFR1; and divalent metal transporter-1, DMT1, also called SLC11A2, DCT1 or NRAMP2), storage (ferritin H, FTH1; and ferritin L, FTL), utilization (erythroid 5′-aminolevulinic acid synthase[16]; mitochondrial aconitase, ACO2; and *Drosophila* succinate dehydrogenase, SDH), and export (ferroportin, FPN, also called SLC40A1, IREG1 or MTP1)[16,17], as well as the cell-cycle control protein CDC14A[18]. Both IRPs independently inhibit translation when bound to an IRE located in the 5′ UTR (for example, in *FTH1*, *FTL*, *ALAS2*, *ACO2* or *SLC40A1*)[19–21], whereas their association with the IREs in the 3′ UTR of *TFRC* mRNA prevents its degradation[22]. The combined IRE-binding activity of both IRPs is high in iron-deficient cells and low in iron-replete cells. Iron-dependent regulation of the IRE-binding activity in combination with the effect of IRP binding to target mRNAs ensures that cells acquire sufficient iron and prevents iron toxicity. Early embryonic lethality in mice lacking both IRPs indicates that the IRP-IRE regulatory network is essential[23]. The phenotypes of mice lacking either IRP1 or IRP2 show that the two IRPs can largely compensate for each other[24],

[1]Molecular Medicine Partnership Unit, Im Neuenheimer Feld 153, 69120 Heidelberg, Germany. [2]European Molecular Biology Laboratory, Meyerhofstrasse 1, 69117 Heidelberg, Germany. [3]Department of Pediatric Oncology, Hematology and Immunology, University of Heidelberg, Im Neuenheimer Feld 153, 69120 Heidelberg, Germany. [4]These authors contributed equally to this work. Correspondence should be addressed to M.W.H. (hentze@embl.de) or M.U.M. (martina.muckenthaler@med.uni-heidelberg.de).

Received 13 November 2006; accepted 27 February 2007; published online 8 April 2007; doi:10.1038/nsmb1222

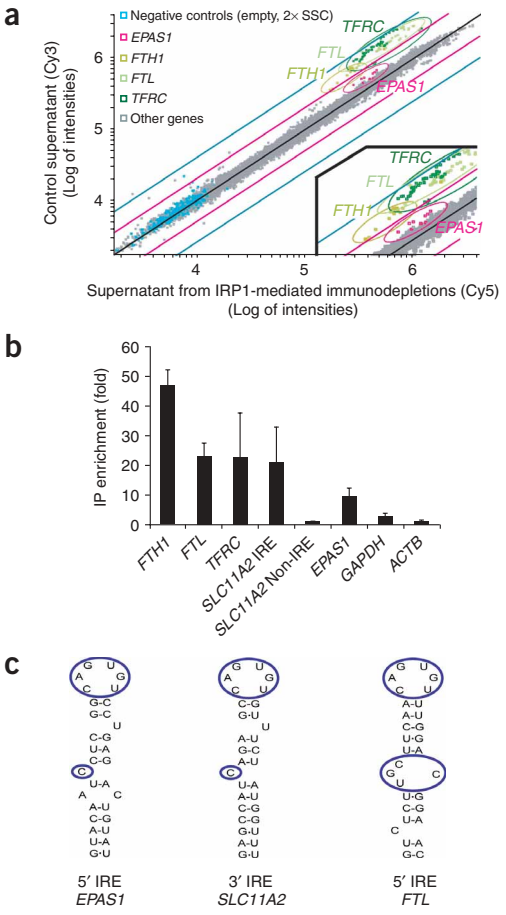

Figure 1 Identification of a novel IRE in the human *EPAS1* mRNA. (**a**) IRE-containing mRNAs were depleted from the supernatant of immunoprecipitations from HeLa cell RNA with an antibody to IRP1 after addition of recombinant IRP1 or buffer (control). RNA from the respective supernatants was analyzed using a dual-color cDNA microarray (IronChip human version 5). Scatterplot shows known IRP target genes (green) and highlights *EPAS1* (magenta) as a previously uncharacterized IRE-containing mRNA. Magenta and blue lines represent two-fold and four-fold depletion ratios. Blue squares represent negative controls such as empty spots or spots containing 2× salt sodium citrate (SSC) buffer. (**b**) qPCR analyses of IRP–mRNP complexes obtained from DFO-treated 786-O cells, showing the expected enrichment of known IRE-containing mRNAs (*FTH1*, *FTL*, *TFRC*, *SLC11A2* IRE) and of the *EPAS1* mRNA. Histogram shows fold enrichment of selected mRNAs in the IRP1 immunoprecipitation (IP) versus the control IP (omitting recombinant IRP1). mRNA levels were normalized to β-actin mRNA (*ACTB*). Data represent averages from three independent experiments. Error bars show s.d. (**c**) Diagram of the IRE structures in the *EPAS1* and *FTL* 5′ UTRs and in the human *SLC11A2* 3′ UTR.

consistent with biochemical results demonstrating that the IREs of the known target mRNAs can bind both IRPs[17].

To date, functional IREs have been identified in a relatively small number of mRNAs. A canonical IRE is composed of a 6-nucleotide apical loop (5′-CAGWGH-3′, where W is adenosine or uridine and H is adenosine, cytosine or uridine) on a stem of five paired nucleotides, a small asymmetrical bulge with an unpaired cytosine on the 5′ strand of the stem and an additional lower stem of variable length[25]. We set out to explore the functional scope of the IRE-IRP regulatory network using a recently described experimental strategy that integrates biochemistry, computational biology and microarray technology to identify new mRNAs that are regulated by the IRE-IRP system[18]. We report the identification and functional characterization of a conserved IRE in the 5′ UTR of the human *EPAS1* mRNA; this IRE mediates iron-dependent control of EPAS1 expression. This discovery highlights a new regulatory link by which iron and oxygen metabolism are coordinately controlled.

RESULTS

An iron-responsive element in the 5′ UTR of *EPAS1* mRNA

We recently devised a method to isolate messenger ribonucleoproteins (mRNPs) that coprecipitate with recombinant IRP1 and to identify their mRNA constituents using microarray technology[18]. When we applied this to RNA from iron-deficient HeLa cells, we clearly observed the expected immunodepletion of known IRE-containing genes (*FTL*, *FTH1* and *TFCR*) from the supernatant (**Fig. 1a**); other known IRE-containing genes (*SLC40A1*, *SLC11A2*, *ALAS2* and *CDC14A*) are expressed at levels below the detection limit in this cell line. In addition to the positive controls, *EPAS1* mRNA is reproducibly depleted as the single novel candidate. This result was confirmed by quantitative PCR (qPCR) analysis of IRP–mRNP complexes isolated from iron-deficient 786-O kidney cells, showing the specific enrichment of this mRNA together with positive controls (**Fig. 1b**). Note that the IRE-containing form, but not the non-IRE isoform, of the *SLC11A2* mRNA is selectively enriched in the IRP1–mRNP complexes, further demonstrating the specificity of the immunopurification procedure. In agreement with the microarray analysis, the *EPAS1* mRNA is substantially (about nine-fold) enriched in IRP1–mRNP complexes. These data suggest the presence of an IRP1-binding site(s) in *EPAS1* mRNA.

Next, we inspected the human *EPAS1* complementary DNA sequence for the presence of putative IREs and detected an IRE-like motif in the 5′ UTR, which is conserved among mammalian species and fish (**Supplementary Fig. 1a** online). This motif has the characteristic 6-nucleotide apical loop (5′-CAGWGH-3′), but it differs from canonical IREs by the presence of an unpaired uridine residue in the upper stem (**Fig. 1c**, compare *EPAS1* 5′ IRE with *FTL* 5′ IRE). Although the IRE of the *SLC11A2* mRNA is similar in this respect (**Fig. 1c** and ref. 26), the *EPAS1* IRE has been missed by *in silico* IRE identification strategies because of the unpaired uridine residue.

Because the distance of a 5′ UTR IRE to the cap structure affects its ability to mediate translational regulation[27,28], we performed rapid amplification of cDNA ends (RACE; **Supplementary Methods** online) using total RNA extracted from HeLa cells to define the *EPAS1* transcription start site. The IRE loop (CAGUGU, underlined C being the first nucleotide of the apical loop, used as a reference point for determination of the position of the IRE) of the human *EPAS1* mRNA is located 85 nucleotides downstream of the 5′ end (**Supplementary Fig. 1b**), an intermediate position between the IREs of the *FTH1* (48 nucleotides[29]) and *SLC40A1* (101 nucleotides[21]) mRNAs. Identical results were obtained for *EPAS1* mRNA from the human 293 kidney cell line (data not shown).

Binding of IRP1 and IRP2 to the *EPAS1* IRE

We next examined the ability of IRP1 and IRP2 to bind the *EPAS1* IRE motif by competitive electrophoretic mobility shift assays (EMSAs). A ^{32}P-labeled *FTH1* IRE probe was incubated with either purified recombinant IRP1 or IRP2, and an increasing amount of unlabeled IRE competitor. As a positive control, the unlabeled wild-type (WT) *FTH1* IRE RNA competes efficiently with the ^{32}P-labeled *FTH1* IRE probe for binding to both IRPs, whereas a mutated competitor RNA

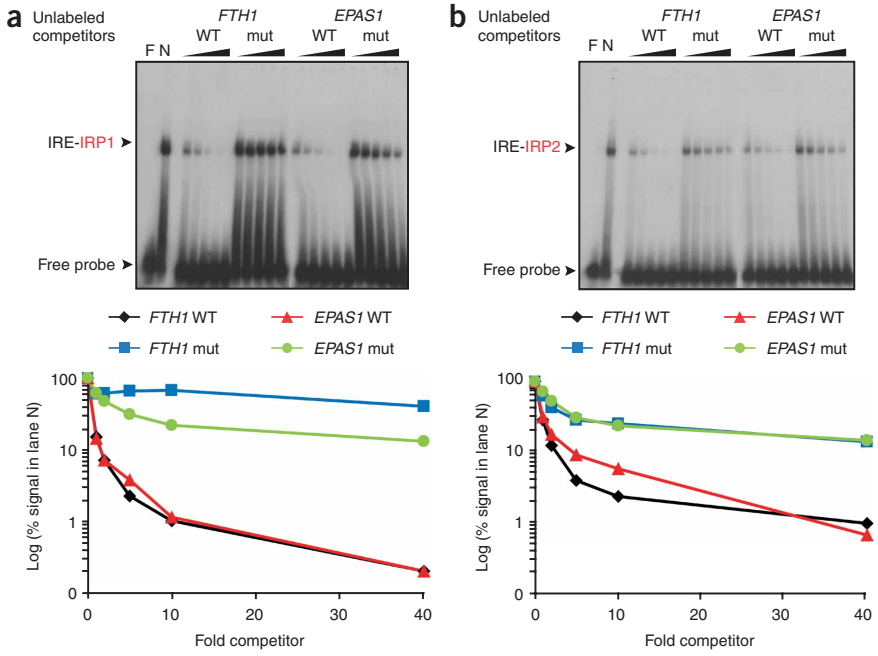

Figure 2 The *EPAS1* IRE binds IRP1 and IRP2. (**a**,**b**) Binding of recombinant human IRP1 (**a**) or IRP2 (**b**) to the *EPAS1* IRE was measured by competitive EMSAs using ^{32}P-labeled *FTH1* IRE probe and an increasing molar excess of unlabeled competitor RNAs: *FTH1* wild-type (WT), *FTH1* cytidine deletion mutant (mut), or *EPAS1* WT or cytidine deletion mutant (mut). Intensity of shifted signal was quantified by phosphorimaging. Data are represented below autoradiographs. F, free probe; N, no competitor added.

with deletion of a cytidine in the IRE loop, as a negative control[20], does not (**Fig. 2**). The unlabeled *EPAS1* IRE competes with the ^{32}P-labeled *FTH1* IRE probe for binding to IRP1 with similar efficiency to that of the *FTH1* IRE, but it competes somewhat less efficiently for IRP2 biding. In both cases, a cytidine deletion in the predicted loop of the *EPAS1* IRE impairs its ability to bind the IRPs (**Fig. 2**). Similar results were obtained using extracts from iron-deficient murine Ltk fibroblasts as a source of endogenous IRPs (data not shown). These data demonstrate that the IRE motif in the 5′ UTR of *EPAS1* mRNA efficiently and specifically binds both IRP1 and IRP2. They also suggest that the *EPAS1* mRNA may be preferentially regulated by IRP1, similar to what it has been reported for *SLC11A2* (ref. 26), which has the most closely structurally related known IRE (**Fig. 1c**).

The *EPAS1* IRE confers iron regulation

To assess the function of *EPAS1* IRE, we fused the complete 5′ UTR of human *EPAS1* mRNA (**Supplementary Fig. 1b**) to the firefly luciferase open reading frame (ORF). The chimeric construct was transiently transfected into 786-O kidney cells that were then treated with an iron chelator (desferrioxamine, DFO) or an iron source (hemin), or left untreated. A *Renilla* luciferase construct was cotransfected to normalize for transfection efficiency. DFO-treated cells show a 34% decrease in luciferase activity compared with untreated cells ($P = 0.0094$), whereas hemin treatment causes about a three-fold increase in luciferase activity ($P = 0.047$) (**Fig. 3a**). This response closely mimics the range of regulation observed for the 5′ UTR of human ferritin H-chain mRNA using an enzymatic reporter assay[29]. As firefly luciferase mRNA levels remain largely unaffected (**Fig. 3b**), the *EPAS1* 5′ UTR confers iron-dependent regulation at the post-transcriptional level. A nearly identical reporter bearing the IRE cytidine deletion (5′EPAS1mut-Luc) is insensitive to changes in iron availability (**Fig. 3**), showing that the IRE is the responsible regulatory element. Notably, the luciferase activity in cells grown in standard media and transfected with the 5′EPAS1mut-Luc construct is about eight-fold higher than in cells transfected with the 5′EPAS1WT-Luc construct (data not shown), whereas the corresponding mRNA levels are the same. This difference implies that the 5′EPAS1WT-Luc construct is strongly repressed under control conditions, probably reflecting an efficient IRE-IRP interaction in the untreated cells. This observation can also explain the modest ability of DFO treatment to further inhibit the expression of the IRE reporter. Similar data were obtained in transfected HeLa cells (**Supplementary Fig. 2** online). We conclude that the motif present in the 5′ UTR of the *EPAS1* mRNA is a bona fide IRE that mediates iron-dependent post-transcriptional regulation.

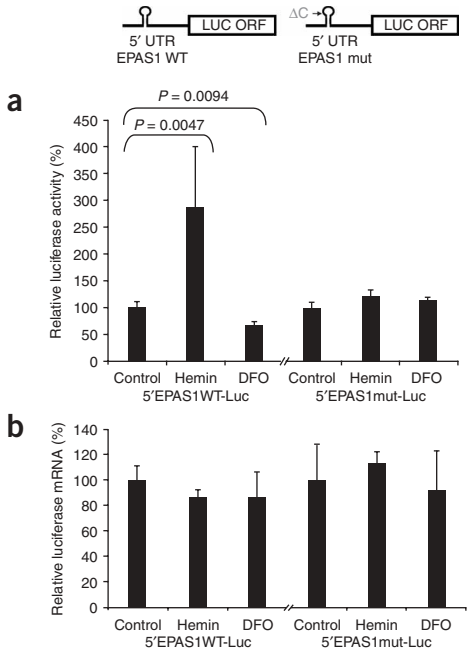

Figure 3 The *EPAS1* IRE mediates iron-dependent post-transcriptional regulation. (**a**) Top, the firefly luciferase ORF was fused to the complete 5′ UTR of the human *EPAS1* mRNA bearing a wild-type or a cytidine deletion mutant IRE and transfected into 786-O cells, together with a *Renilla* luciferase construct (as a control for transfection efficiency). Transfected cells were treated for 8 h with DFO or hemin, or were untreated (control). Bottom, histogram showing firefly luciferase activity normalized to *Renilla* luciferase activity. (**b**) Firefly and *Renilla* luciferase mRNA levels determined by qPCR. Histogram shows firefly luciferase mRNA levels normalized to *Renilla* luciferase mRNA. In **a** and **b**, data represent averages from three independent samples; error bars show s.d.; values obtained from untreated cells (control) were set to 100%; *P* values (Student's *t*-test) are shown when $P < 0.05$.

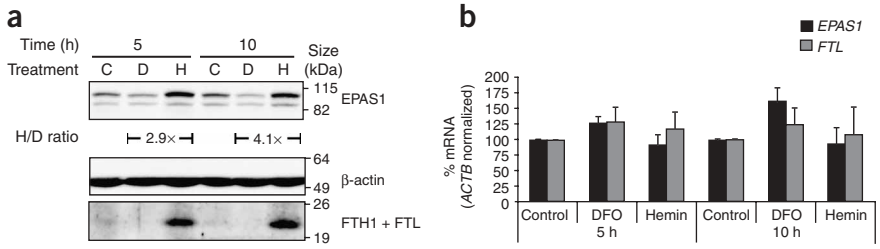

Figure 4 Post-transcriptional regulation of EPAS1 expression by iron. VHL-deficient 786-O cells were treated with DFO (D) or hemin (H), or were left untreated (control, C) for 5 or 10 h. (**a**) EPAS1, β-actin and ferritin (FTH1 + FTL) protein levels were determined by immunoblot analysis of total protein extracts. Expression ratio in hemin- and DFO-treated cells (H/D) is indicated. Representative immunoblot is shown from three independent experiments. (**b**) *EPAS1* and *FTL* mRNA levels were assayed by qPCR. Histogram shows averages from three independent samples after normalization to *ACTB*. Error bars show s.d. Values obtained from untreated cells (control) were set to 100%.

Iron regulation of *EPAS1* translation

The experiments in **Figure 3** show that the 5′ UTR IRE of the *EPAS1* mRNA represses reporter mRNA expression in iron-deficient cells. This could provide a previously unrecognized mechanism for negative-feedback regulation of EPAS1. To distinguish between the post-translational regulation of EPAS1 by oxygen- and iron-dependent hydroxylases[9] and IRE-mediated post-transcriptional regulation, we took advantage of the 786-O renal carcinoma cell line, in which EPAS1 proteasomal degradation is prevented by VHL deficiency[30]. 786-O cells were treated with DFO or hemin, or were left untreated, and *EPAS1* mRNA and protein expression were analyzed after 5 and 10 h. Ferritin expression was assayed as a positive control for iron regulation. As expected, hemin treatment markedly increases ferritin protein (**Fig. 4a**, FTH1 + FTL) but not mRNA levels (**Fig. 4b**, FTL). Although the change is quantitatively less, EPAS1 protein expression is also enhanced upon hemin treatment and decreased upon DFO exposure (**Fig. 4a**). *EPAS1* mRNA levels do not mirror the changes in EPAS1 protein expression (**Fig. 4b**), showing that iron regulates endogenous EPAS1 expression post-transcriptionally. Similar results were obtained in a different human renal carcinoma cell line, RC1 (**Supplementary Fig. 3a**,**b** online), where we also monitored HIF1α protein levels (786-O cells do not express HIF1α) and did not observe variations in response to iron perturbation (**Supplementary Fig. 3c**).

To analyze *EPAS1* mRNA translation directly, we treated HeLa cells with DFO or hemin and determined the polysomal association of *EPAS1* mRNA using sucrose gradients (**Fig. 5**). As a negative control for iron regulation, we analyzed β-actin mRNA (*ATCB*) from the same fractions. Approximately 80% of the *ATCB* mRNA is present in dense, polysomal fractions, and this percentage is independent of the iron status of the cell (**Fig. 5b**). In contrast, the distribution of the *EPAS1* mRNA in polysomal (P) versus nonpolysomal (NP) fractions changes profoundly, with more actively translated mRNA in hemin-treated cells (P/NP ratio 2.86 ± 1.5) than in DFO-treated cells (P/NP ratio 1.10 ± 0.2) (**Fig. 5b**). This change in the distribution of the *EPAS1* mRNA between the P and the NP fractions mirrors the regulation of the *FTH1* and *FTL* mRNAs, two IRE-regulated mRNAs that strongly shift between P and NP fractions (data not shown).

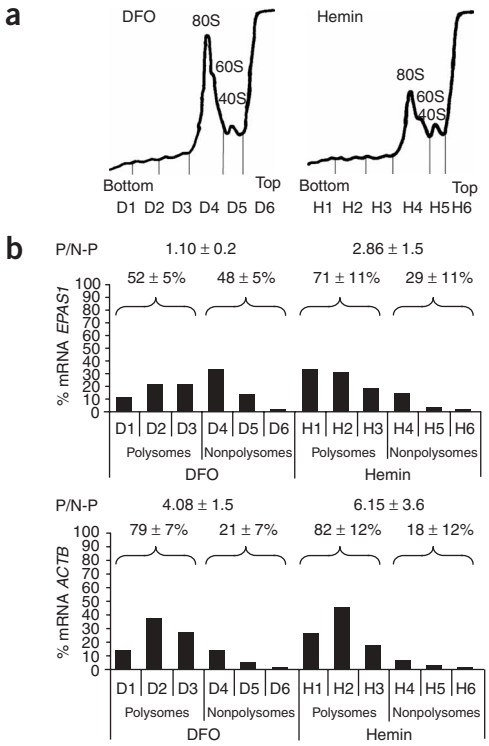

Figure 5 Polysome analysis of *EPAS1* and *ACTB* mRNA translation in response to iron treatment. HeLa cells were incubated for 8 h with DFO (D) or hemin (H), and cytoplasmic extracts were fractionated from 10%–40% sucrose density gradients. (**a**) Representative A_{264} profile. Fractions corresponding to mRNPs (D6, H6), 40S subunit (D5, H5), 60S and 80S subunits (D4, H4) and polysomes (D1–D3, H1–H3) are indicated. (**b**) qPCR analysis of *EPAS1* and *ACTB* mRNAs in the different fractions. For each treatment, the mRNA level in each fraction was calculated as a percentage of the total; data from a representative experiment is plotted. Distributions of *EPAS1* and *ACTB* mRNAs in polysomes (D1–D3, H1–H3) versus nonpolysomes (D4–D6, H4–H6) were calculated from three independent samples, for which qPCR analyses were done in triplicate, and are represented above graph as mean ± s.d. Polysome to nonpolysome ratio (P/NP) is also indicated.

DISCUSSION

In this report, we identify and characterize a phylogenetically conserved IRE in the 5′ UTR of the *EPAS1* mRNA, which controls *EPAS1* translation in response to iron. These results uncover a previously unrecognized mechanism for feedback regulation between iron and oxygen metabolism.

Post-translational regulation of HIFα by iron- and oxygen-dependent hydroxylases (PDH1, PDH2, PDH3 and FIH-1) is a major mechanism for coupling oxygen sensing with the activation of hypoxia response genes via HIF1 in higher organisms[9]. The fine-tuning of HIFα levels is important and complex, and it involves multiple steps of intervention. These include a post-transcriptional mechanism for the down-regulation of *HIF1A* (the HIF1α gene) involving mTOR inhibition by the promyelocytic leukemia (PML) protein[31]; moreover, the *HIF1A* mRNA bears an internal ribosome entry sequence in its 5′ UTR, which allows translation under conditions that are inhibitory to cap-dependent translation, such as hypoxia[32]. HIF1α activity is also controlled by nuclear-cytoplasmic localization[33]. Our study reveals the only presently known mechanism to limit EPAS1 expression during iron deficiency.

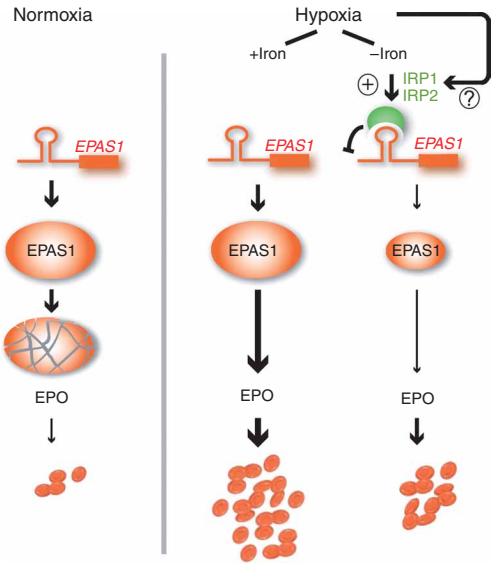

Figure 6 Proposed model for the feedback regulation between iron and oxygen metabolism via the IRE-IRP regulatory system and the 5′ UTR IRE of *EPAS1* mRNA. See text for details. Question mark at top right denotes that reports on the effect of hypoxia on the IRPs in cultured cells have been contradictory[48–50].

Although the two HIFα transcription factors bind the same HRE sequences of target genes *in vitro*[4,34], *in vivo* studies indicate that HIF1α and EPAS1 modulate the transcription of an overlapping but distinct set of target genes[13–15]. The different HIFα isoforms also show differences in their expression patterns: HIF1α is expressed ubiquitously, whereas EPAS1 is important in endothelial cells[7] as well as in bone marrow macrophages, kidney epithelial cells, liver parenchyma, cardiac myocytes, uterine decidual cells and pancreatic parenchymal cells[35]. Whereas Hif1α-deficient mice die *in utero* owing to aberrant vasculature[36], Epas1 deficiency causes phenotypic abnormalities that range, depending on the genetic background, from embryonic or perinatal lethality associated with defects in vascular remodeling[37], catecholamine production[38], or lung maturation[39] to impaired oxygen homeostasis in mice that survive until early adulthood[40]. Notably, Epas1 regulates murine hematopoiesis in an erythropoietin (EPO)-dependent manner[40,41], and mice carrying *Epas1* hypomorphic alleles suffer from retinal degeneration associated with decreased *Epo* mRNA levels[42,43]. These data point toward a specific role of EPAS1 in EPO regulation.

Epas1 expression is increased in EPO-producing kidney interstitial fibroblasts of rats subjected to hypoxia, whereas Hif1α is the dominant form in tubular epithelial cells[44]. Short interfering RNA knockdown experiments in Hep3B and Kelly cells have shown that the *EPO* gene is selectively activated by EPAS1 rather than HIF1α[14]. On the basis of our findings and the above literature reports, we propose that iron regulation of *EPAS1* translation can serve to modulate EPO levels, thereby adjusting the rate of red blood cell production (that is, iron utilization) to iron availability (**Fig. 6**). EPAS1 is degraded by the proteasome in normoxic cells, whereas it is stable during hypoxia, stimulating EPO synthesis and enhancing erythropoiesis. When iron levels are adequate and meet the demand of increased heme synthesis, the mechanism controlling EPAS1 protein stability serves physiologic needs. However, under conditions of iron deficiency, stimulation of erythropoiesis would lead to the accumulation of hypochromic and microcytic red blood cells, as iron is crucial for heme synthesis and hemoglobin production. To avoid such a situation, EPO stimulation of erythropoiesis should be diminished under low-oxygen conditions when iron is limiting. We propose that this can be achieved by the IRE-IRP system, which would attenuate translation of *EPAS1* via its 5′ UTR IRE and allow negative-feedback control when iron is scarce.

METHODS

Cell culture and treatments. Cells were grown in 5% CO_2 at 37 °C in DMEM supplemented with 10% (v/v) FBS, 1% (w/v) L-glutamine, 1% (v/v) penicillin and 1% (v/v) streptomycin (HeLa cells), or in RPMI 1,640 medium supplemented with 10% (v/v) FBS, 1% (v/v) penicillin and 1% (v/v) streptomycin (786-O cells). Cells were treated with 100 μM DFO (Sigma) or 100 μM hemin (Leiras Oy), as indicated.

Plasmids. The plasmids for the synthesis of wild-type and mutant ferritin H-chain EMSA probes were described previously[18,45]. The *EPAS1* IRE templates were generated by swapping the ferritin H-chain IRE sequence in the I-12.CAT plasmid[45] with annealed synthetic oligonucleotides comprising the *EPAS1* IRE sequence (EPAS1wtIRE-sense and EPAS1wtIRE-reverse for the wild-type IRE construct; EPAS1mutIRE-forward and EPAS1mutIRE-reverse for the mutant IRE; **Supplementary Table 1** online). The templates were linearized with XbaI and used for *in vitro* transcription using the T7 RNA polymerase (Stratagene) as described[18].

Firefly luciferase chimeric constructs were generated by inserting a fusion of the entire *EPAS1* 5′ UTR with the luciferase firefly ORF into pcDNA3 (Invitrogen), to generate the 5′EPAS1wt-Luc plasmid. The corresponding mutant IRE construct (5′EPAS1mut-Luc) was generated by swapping the AfeI-BlpI sequence of the *EPAS1* 5′ UTR with annealed synthetic oligonucleotides (EPAS1mutIRE-AfeI/BlpI-forward and EPAS1mutIRE-AfeI/BlpI-reverse; **Supplementary Table 1**). As a control for transfection efficiency, we used a pCDNA3 vector bearing the *Renilla* luciferase ORF.

Transfections and dual luciferase reporter assays. 786-O cells were seeded at a density of 3×10^4 cells per well in 24-well plates and transfected 24 h later with 150 ng of 5′EPAS1wt-Luc or 5′EPAS1mut-Luc plasmids (together with 50 ng of pcDNA3-*Renilla* plasmid) using Effectene (Qiagen). Cells were washed 24 h later and incubated with medium containing either DFO, hemin or no reagent. Luciferase activities were determined using the dual luciferase assay kit (Promega) and a LB 96V microplate luminometer (Berthold Technologies).

Preparation of cell lysates and immunoblotting. Cells were lysed in 20 mM Tris (pH 7.5), 150 mM NaCl, 10 mM EDTA, 2% (w/v) SDS supplemented with a complete protease inhibitor cocktail (Roche). The lysates were sonicated and debris was pelleted by centrifugation. Total protein concentration was determined using the DC protein assay kit (Bio-Rad). Equal amounts of protein were resolved by SDS-PAGE (11% acrylamide) and transferred onto polyvinylidene difluoride membranes (Millipore). The membranes were blocked in TBST containing 5% (w/v) dry milk and incubated with rabbit polyclonal antibodies to HIF2α (NB100-122, Novus) or ferritin (Roche), or with a mouse monoclonal antibody to β-actin (A-5441, Sigma). Immunocomplexes were revealed using secondary antibodies to rabbit or mouse conjugated to horseradish peroxidase (Amersham Biosciences), together with the ECL (PerkinElmer) or the Femto (Pierce) chemiluminescence detection system.

Electrophoretic mobility shift assays. EMSAs were done as described[18,20]. Briefly, a [^{32}P]UTP-labeled human *FTH1* IRE probe (600,000 c.p.m.) was incubated with 10 ng of purified recombinant human IRP1 or IRP2 protein for 15 min at 25 °C in the presence of excess unlabeled competitor RNA as indicated. RNA–protein complexes were resolved by nondenaturing PAGE and visualized using a fluorimager (Fujifilm FLA-2000, Amersham Biosciences).

Polysome analysis. Cytoplasmic extracts were prepared from HeLa cells and fractionated by ultracentrifugation through linear sucrose gradients (10%–40% w/v) as described[46]. Fractions corresponding to polysomes (fractions 1, 2 and 3) or to the 80S and 60S subunits, the 40S subunit and the mRNPs

(nonpolysome fractions 4, 5 and 6) were collected and RNA was isolated from each fraction by proteinase K digestion followed by phenol and phenol-chloroform extractions and isopropanol precipitation.

Immunoprecipitations and microarray experiments. Immunoprecipitations and microarray experiments were done as described[18]. Microarray dye-switch experiments were done to exclude possible artifacts associated with uneven incorporation of cyanine dyes into cDNAs[47].

RNA extraction and quantitative real-time reverse-transcription PCR analyses. Total RNA was extracted from 786-O cells using Trizol (Invitrogen), and 2 μg was used for first-strand synthesis of cDNAs with random hexamers and the Superscript II reverse transcriptase (Invitrogen). RNA extracted from 786-O cells transfected with firefly and *Renilla* luciferase plasmids was further digested with RQ1 RNase-free DNase (Promega) at 37 °C for 1 h before reverse transcription. qPCR was done using SYBR-green and an ABI 7500 sequence-detection system instrument and software (Applied Biosystems). The data reported represent averages from three independent RNA samples for which qPCR analyses were done in triplicate. The level of each RNA was normalized to the corresponding level of *ACTB* mRNA (when assaying *FTL* and *EPAS1* mRNA expression) or *Renilla* luciferase mRNA (when assaying firefly luciferase mRNA expression). The data are expressed as a percentage of the value in the control (untreated) sample.

qPCR analysis of IRP–IRE mRNP complexes was done as described[18]. mRNA levels were determined for three independent immunopurification experiments, for which each qPCR analysis was done in triplicate. For qPCR of sucrose gradient fractions, one tenth of each fraction was used for reverse transcription. The primers used in qPCR analyses are listed in **Supplementary Table 1**.

Statistics. Student's *t*-test (two tails and two samples with equal variance) was used to compare luciferase activity values between control and hemin-treated cells or control and DFO-treated cells. *P*-values are reported when $P < 0.05$.

Note: Supplementary information is available on the Nature Structural & Molecular Biology website.

ACKNOWLEDGMENTS

We thank Y. Vainshtein for support with microarray data analysis, J. Stolte for maintenance of the IronChip platform, V. Benes and members of the European Molecular Biology Laboratory Genomics Core Facility for help with qPCR and sequencing, and D. Shouval (Hadassah University Hospital) for kindly providing the RC1 renal carcinoma cell line. This work was supported by grants from the Marie Curie Quality of Life Programme, CORDIS FP5 (QLGA-CT-2001-52011) and the Young Investigator Award of the Medical Faculty, University of Heidelberg to M.S., by grants from the Forschungsschwerpunktprogramm des Landes Baden-Württemberg (RNA and disease) to M.U.M. and M.W.H. and by funds from the Gottfried Wilhem Leibniz Prize to M.W.H.

AUTHOR CONTRIBUTIONS

M.S., B.G., M.U.M. and M.W.H designed and analyzed the experiments and wrote the paper. M.S. and B.G. performed the experiments.

COMPETING INTERESTS STATEMENT

The authors declare no competing financial interests.

Published online at http://www.nature.com/nsmb
Reprints and permissions information is available online at http://npg.nature.com/reprintsandpermissions

1. Eckardt, K.U. & Kurtz, A. Regulation of erythropoietin production. *Eur. J. Clin. Invest.* **35** Suppl. 3, 13–19 (2005).
2. Leung, P.S., Srai, S.K., Mascarenhas, M., Churchill, L.J. & Debnam, E.S. Increased duodenal iron uptake and transfer in a rat model of chronic hypoxia is accompanied by reduced hepcidin expression. *Gut* **54**, 1391–1395 (2005).
3. Wang, G.L., Jiang, B.H., Rue, E.A. & Semenza, G.L. Hypoxia-inducible factor 1 is a basic-helix-loop-helix-PAS heterodimer regulated by cellular O2 tension. *Proc. Natl. Acad. Sci. USA* **92**, 5510–5514 (1995).
4. Ema, M. *et al.* A novel bHLH-PAS factor with close sequence similarity to hypoxia-inducible factor 1alpha regulates the VEGF expression and is potentially involved in lung and vascular development. *Proc. Natl. Acad. Sci. USA* **94**, 4273–4278 (1997).
5. Flamme, I. *et al.* HRF, a putative basic helix-loop-helix-PAS-domain transcription factor is closely related to hypoxia-inducible factor-1 alpha and developmentally expressed in blood vessels. *Mech. Dev.* **63**, 51–60 (1997).
6. Hogenesch, J.B. *et al.* Characterization of a subset of the basic-helix-loop-helix-PAS superfamily that interacts with components of the dioxin signaling pathway. *J. Biol. Chem.* **272**, 8581–8593 (1997).
7. Tian, H., McKnight, S.L. & Russell, D.W. Endothelial PAS domain protein 1 (EPAS1), a transcription factor selectively expressed in endothelial cells. *Genes Dev.* **11**, 72–82 (1997).
8. Wenger, R.H. & Gassmann, M. Oxygen(es) and the hypoxia-inducible factor-1. *Biol. Chem.* **378**, 609–616 (1997).
9. Schofield, C.J. & Ratcliffe, P.J. Oxygen sensing by HIF hydroxylases. *Nat. Rev. Mol. Cell Biol.* **5**, 343–354 (2004).
10. Kallio, P.J., Wilson, W.J., O'Brien, S., Makino, Y. & Poellinger, L. Regulation of the hypoxia-inducible transcription factor 1alpha by the ubiquitin-proteasome pathway. *J. Biol. Chem.* **274**, 6519–6525 (1999).
11. Lando, D., Peet, D.J., Whelan, D.A., Gorman, J.J. & Whitelaw, M.L. Asparagine hydroxylation of the HIF transactivation domain a hypoxic switch. *Science* **295**, 858–861 (2002).
12. Semenza, G.L. Hypoxia-inducible factor 1: oxygen homeostasis and disease pathophysiology. *Trends Mol. Med.* **7**, 345–350 (2001).
13. Hu, C.J., Wang, L.Y., Chodosh, L.A., Keith, B. & Simon, M.C. Differential roles of hypoxia-inducible factor 1alpha (HIF-1alpha) and HIF-2alpha in hypoxic gene regulation. *Mol. Cell. Biol.* **23**, 9361–9374 (2003).
14. Warnecke, C. *et al.* Differentiating the functional role of hypoxia-inducible factor (HIF)-1alpha and HIF-2alpha (EPAS-1) by the use of RNA interference: erythropoietin is a HIF-2alpha target gene in Hep3B and Kelly cells. *FASEB J.* **18**, 1462–1464 (2004).
15. Smith, K. *et al.* Silencing of epidermal growth factor receptor suppresses hypoxia-inducible factor-2-driven VHL–/– renal cancer. *Cancer Res.* **65**, 5221–5230 (2005).
16. Hentze, M.W., Muckenthaler, M.U. & Andrews, N.C. Balancing acts: molecular control of mammalian iron metabolism. *Cell* **117**, 285–297 (2004).
17. Wallander, M.L., Leibold, E.A. & Eisenstein, R.S. Molecular control of vertebrate iron homeostasis by iron regulatory proteins. *Biochim. Biophys. Acta* **1763**, 668–689 (2006).
18. Sanchez, M. *et al.* Iron regulation and the cell cycle: identification of an iron-responsive element in the 3′-untranslated region of human cell division cycle 14A mRNA by a refined microarray-based screening strategy. *J. Biol. Chem.* **281**, 22865–22874 (2006).
19. Muckenthaler, M., Gray, N.K. & Hentze, M.W. IRP-1 binding to ferritin mRNA prevents the recruitment of the small ribosomal subunit by the cap-binding complex eIF4F. *Mol. Cell* **2**, 383–388 (1998).
20. Gray, N.K., Pantopoulos, K., Dandekar, T., Ackrell, B.A. & Hentze, M.W. Translational regulation of mammalian and *Drosophila* citric acid cycle enzymes via iron-responsive elements. *Proc. Natl. Acad. Sci. USA* **93**, 4925–4930 (1996).
21. Liu, X.B., Hill, P. & Haile, D.J. Role of the ferroportin iron-responsive element in iron and nitric oxide dependent gene regulation. *Blood Cells Mol. Dis.* **29**, 315–326 (2002).
22. Binder, R. *et al.* Evidence that the pathway of transferrin receptor mRNA degradation involves an endonucleolytic cleavage within the 3′ UTR and does not involve poly(A) tail shortening. *EMBO J.* **13**, 1969–1980 (1994).
23. Smith, S.R., Ghosh, M.C., Ollivierre-Wilson, H., Hang Tong, W. & Rouault, T.A. Complete loss of iron regulatory proteins 1 and 2 prevents viability of murine zygotes beyond the blastocyst stage of embryonic development. *Blood Cells Mol. Dis.* **36**, 283–287 (2006).
24. Galy, B., Ferring, D. & Hentze, M.W. Generation of conditional alleles of the murine Iron Regulatory Protein (IRP)-1 and -2 genes. *Genesis* **43**, 181–188 (2005).
25. Hentze, M.W. *et al.* A model for the structure and functions of iron-responsive elements. *Gene* **72**, 201–208 (1988).
26. Gunshin, H. *et al.* Iron-dependent regulation of the divalent metal ion transporter. *FEBS Lett.* **509**, 309–316 (2001).
27. Goossen, B. & Hentze, M.W. Position is the critical determinant for function of iron-responsive elements as translational regulators. *Mol. Cell. Biol.* **12**, 1959–1966 (1992).
28. Paraskeva, E., Gray, N.K., Schlager, B., Wehr, K. & Hentze, M.W. Ribosomal pausing and scanning arrest as mechanisms of translational regulation from cap-distal iron-responsive elements. *Mol. Cell. Biol.* **19**, 807–816 (1999).
29. Hentze, M.W. *et al.* Identification of the iron-responsive element for the translational regulation of human ferritin mRNA. *Science* **238**, 1570–1573 (1987).
30. Maxwell, P.H. *et al.* The tumour suppressor protein VHL targets hypoxia-inducible factors for oxygen-dependent proteolysis. *Nature* **399**, 271–275 (1999).
31. Bernardi, R. *et al.* PML inhibits HIF-1alpha translation and neoangiogenesis through repression of mTOR. *Nature* **442**, 779–785 (2006).
32. Lang, K.J., Kappel, A. & Goodall, G.J. Hypoxia-inducible factor-1alpha mRNA contains an internal ribosome entry site that allows efficient translation during normoxia and hypoxia. *Mol. Biol. Cell* **13**, 1792–1801 (2002).
33. Kallio, P.J. *et al.* Signal transduction in hypoxic cells: inducible nuclear translocation and recruitment of the CBP/p300 coactivator by the hypoxia-inducible factor-1alpha. *EMBO J.* **17**, 6573–6586 (1998).

34. Semenza, G.L. *et al.* Hypoxia response elements in the aldolase A, enolase 1, and lactate dehydrogenase A gene promoters contain essential binding sites for hypoxia-inducible factor 1. *J. Biol. Chem.* **271**, 32529–32537 (1996).
35. Wiesener, M.S. *et al.* Widespread hypoxia-inducible expression of HIF-2alpha in distinct cell populations of different organs. *FASEB J.* **17**, 271–273 (2003).
36. Ryan, H.E., Lo, J. & Johnson, R.S. HIF-1 alpha is required for solid tumor formation and embryonic vascularization. *EMBO J.* **17**, 3005–3015 (1998).
37. Peng, J., Zhang, L., Drysdale, L. & Fong, G.H. The transcription factor EPAS-1/hypoxia-inducible factor 2alpha plays an important role in vascular remodeling. *Proc. Natl. Acad. Sci. USA* **97**, 8386–8391 (2000).
38. Tian, H., Hammer, R.E., Matsumoto, A.M., Russell, D.W. & McKnight, S.L. The hypoxia-responsive transcription factor EPAS1 is essential for catecholamine homeostasis and protection against heart failure during embryonic development. *Genes Dev.* **12**, 3320–3324 (1998).
39. Compernolle, V. *et al.* Loss of HIF-2alpha and inhibition of VEGF impair fetal lung maturation, whereas treatment with VEGF prevents fatal respiratory distress in premature mice. *Nat. Med.* **8**, 702–710 (2002).
40. Scortegagna, M., Morris, M.A., Oktay, Y., Bennett, M. & Garcia, J.A. The HIF family member EPAS1/HIF-2alpha is required for normal hematopoiesis in mice. *Blood* **102**, 1634–1640 (2003).
41. Scortegagna, M. *et al.* HIF-2alpha regulates murine hematopoietic development in an erythropoietin-dependent manner. *Blood* **105**, 3133–3140 (2005).
42. Morita, M. *et al.* HLF/HIF-2alpha is a key factor in retinopathy of prematurity in association with erythropoietin. *EMBO J.* **22**, 1134–1146 (2003).
43. Ding, K., Scortegagna, M., Seaman, R., Birch, D.G. & Garcia, J.A. Retinal disease in mice lacking hypoxia-inducible transcription factor-2alpha. *Invest. Ophthalmol. Vis. Sci.* **46**, 1010–1016 (2005).
44. Rosenberger, C. *et al.* Expression of hypoxia-inducible factor-1alpha and -2alpha in hypoxic and ischemic rat kidneys. *J. Am. Soc. Nephrol.* **13**, 1721–1732 (2002).
45. Gray, N.K. *et al.* Recombinant iron-regulatory factor functions as an iron-responsive-element-binding protein, a translational repressor and an aconitase. A functional assay for translational repression and direct demonstration of the iron switch. *Eur. J. Biochem.* **218**, 657–667 (1993).
46. Korner, C.G. *et al.* The deadenylating nuclease (DAN) is involved in poly(A) tail removal during the meiotic maturation of *Xenopus* oocytes. *EMBO J.* **17**, 5427–5437 (1998).
47. Benes, V. & Muckenthaler, M. Standardization of protocols in cDNA microarray analysis. *Trends Biochem. Sci.* **28**, 244–249 (2003).
48. Hanson, E.S., Foot, L.M. & Leibold, E.A. Hypoxia post-translationally activates iron-regulatory protein 2. *J. Biol. Chem.* **274**, 5047–5052 (1999).
49. Toth, I., Yuan, L., Rogers, J.T., Boyce, H. & Bridges, K.R. Hypoxia alters iron-regulatory protein-1 binding capacity and modulates cellular iron homeostasis in human hepatoma and erythroleukemia cells. *J. Biol. Chem.* **274**, 4467–4473 (1999).
50. Christova, T. & Templeton, D.M. Effect of hypoxia on the binding and subcellular distribution of iron regulatory proteins. *Mol. Cell. Biochem.,* published online 3 January 2007.